International Conference on Space Optics—ICSO 2018

Chania, Greece

9–12 October 2018

Edited by Zoran Sodnik, Nikos Karafolas, and Bruno Cugny

Binary blazed reflection grating for UV/VIS/NIR/SWIR spectral range

Frank Burmeister

Thomas Flügel-Paul

Uwe Zeitner

Mane-Si-Laure Lee Bouhours

et al.

esa icso proceedings cnes

International Conference on Space Optics — ICSO 2018, edited by Zoran Sodnik, Nikos Karafolas, Bruno Cugny, Proc. of SPIE Vol. 11180, 111801J · © 2018 ESA and CNES · CCC code: 0277-786X/18/$18 · doi: 10.1117/12.2535974

Binary blazed reflection grating for UV/VIS/NIR/SWIR spectral range

Frank Burmeister [a], Thomas Flügel-Paul*[a], Uwe D. Zeitner[a], Mane-Si-Laure Lee Bouhours[b], Gaëlle Lehoucq[b], Julie Cholet[b], Brigitte Loiseaux[b], Nicolas Tetaz[c], Roman Windpassinger[d], Matteo Taccola[d],

[a]Fraunhofer Institute for Applied Optics and Precision Engineering, Albert-Einstein-Strasse 7, 07745 Jena, Germany; [b]Thales Research & Technology, 1 Av Fresnel, 91767 Palaiseau, France; [c]Thales Alenia Space, 5 Allée des Gabians, BP 99, 06156 Cannes la Bocca Cedex, France, [d]European Space Agency (ESA), European Space Research and Technology Centre (ESTEC), Postbus 299-2200 AG Noordwijk, The Netherlands

ABSTRACT

We report on the design and fabrication of a reflection grating for hyperspectral applications operating in the range from 340 nm to 1040 nm wavelength. The blazed grating is based on an effective medium approach, where the desired functionality is realized using a binary surface relief structure. For each period, a gradient in size of the local grating features mimics an interface which adds a linear phase profile to the illuminating beam – thus introducing diffraction. The surface relief structure is composed of 2D structures - pillars with diameters from 200 nm to 350 nm to voids with diameters from 300nm to 120 nm. Overall, an entire number of ~50 such features are arranged to establish an overall unit cell of the grating over a length of 30 µm. By purposeful design of size, shape and arrangement of the sub-wavelength features such gratings offer novel opportunities in tailoring the spectral response, i.e. particular broadband efficiency or the enhancement of the efficiency in specific sub-domains of the spectrum. We will present measured performance results of a grating covering a circular area of 80mm in diameter manufactured on a 4inch-wafer. Finally, we will give an outlook on how such structures can be applied to curved surfaces and even ultra-broadband operation.

Keywords: diffraction grating, imaging spectroscopy, hyperspectral imaging, concave mirror, electron beam lithography, subwavelength structures, effective index media, artificial anisotropy.

1. INTRODUCTION

Hyperspectral imaging missions aim for studying environmental changes, ecosystems' responses to human influences, or monitor the management of essential natural resources. Broadband spectroscopic images allow to determine various diagnostic parameters in order to quantify, e.g., the state of environmental changes in earth's ecosystems or they allow to monitor the usage and lifecycle of natural resources. Space-born technology demonstrators like Hyperion (NASA), CHRIS (ESA), HJ-1A (CASC) and HICO (NASA) are already in operation while other instruments such as EnMAP, HyspIRI and CHIME are currently in different phases of development[1,2].

For the next generation of hyperspectral instrumentation for space-born earth observation missions, reduction of optical modules is a main objective. Besides a beneficial impact on mass and volume of the instruments, co-registration could be improved and calibration simplified. For the realization of such instruments, the diffraction grating is a critical component, since high diffraction efficiency and minimum polarization sensitivity over wide spectral range are required.

Here we report on our effort to realize prototype gratings covering a circular area with diameter of ~80mm manufactured on a 4-inch silicon substrate. We start with a substrate's front surface that is coated by a broadband reflective layer stack of protected aluminum with a top layer consisting of silicon dioxide (SiO_2). The grating structure is determined by electron beam lithography in combination with reactive ion etching. Binary features, i.e. pillars and holes/voids, of purposefully designed feature size realize the diffraction effect. The pillars have diameters from 200 nm to 350 nm and the voids have diameters from 300nm down to 120 nm. Overall, an entire number of ~50 such features are arranged to establish a single unit cell of the grating over a length of 30 µm.

The paper is organized as follows: In Section 2 we briefly outline the grating design and geometry. In Section 3 we report on the grating manufacturing process. The performance of the first prototype on a flat substrate will be proven by optical measurements presented in Section 4. The paper ends with an outlook on how to achieve equivalent structures on moderately curved surfaces and on ultra-broadband operation covering the full bandwidth from 340nm up to 2500nm.

*thomas.fluegel-paul@iof.fraunhofer.de; phone +49 3641 807434; www.iof.fraunhofer.de

2. GRATING DESIGN

Hyperspectral imaging instruments with a large spectral range require low-dispersive gratings operating in first order while achieving a high throughput over the entire bandwidth. Depending on the spectrometer's design the grating may be implemented on plane or curved substrate or is operated near normal or oblique incidence[4,5]. Despite all differences, there exist also common parameters. Nearly all optical designs rely on reflection gratings. The required grating periods are somewhere around 20µm or 30µm. A comprehensive overview and trade-off study can be found for example in Ref. [5].

The current development project aims at the realization of a grating whose specification is inspired by a particular optical design of a Dyson spectrometer[2]. The period is 30µm and the nominal angle of incidence is 0.5°. The required minimum throughput lies only between 35% and 50%, however, it must be achieved throughout the entire spectrum between 340nm and 1040nm. The first choice will be to use ordinary blazed gratings with a continuous saw-tooth profile. On the one hand, such gratings achieve peak efficiencies up to approximately 90% (depending on the reflector material), but go down quite rapidly when approaching the band edges in the UV and NIR region. Moreover, taking into account manufacturing tolerances (e.g. imperfect profiles like corner rounding) then an ordinary saw-tooth grating appears to be a bad choice if the spectral bandwidth exceeds one octave. In consequence, one has to look for alternative approaches. Binary gratings where the blazing functionality is achieved via sub-wavelength features have been demonstrated to be a promising alternative[6,7,8]. Moreover, by a dedicated design of the sub-wavelength features' sizes the spectral response can be either broadened or it can be tuned in order to emphasize particular spectral regions of interest.

In order to meet the requirements on a broadband operation, we have designed a diffractive nano-structure with a total number of 50 sub-wavelength entities constituting a unit cell of the overall grating (see Figure1a). The design of the grating is based on artificial material engineering[7]. The reflection is realized by an underlying protected aluminum layer and the actual grating structure is applied on top. The idea is to realize an increasing effective refractive index throughout the unit cell of the grating (from left to right) which then transforms into a linear phase added to the incident beam. A sketch of the structural layout is provided by Figure 1a. The lowest refractive index is achieved on the left (see Figure 1a) where only small pillars made of SiO_2 rise on the underlying reflection layer. The size (width) of the pillars is increasing before the topology of the structure turns into voids/holes which are "drilled" into a silicon oxide-background layer. The right most part of the grating's unit cell contains a large lamella of SiO_2 exhibiting the highest (effective) refractive index. The pitch between neighboring features (pillars or voids) is 500nm in both lateral directions and the depth of the structure is 600nm. Finally, the calculated diffraction efficiency of this structure, illuminated under non-polarized light (average efficiencies under illumination in TE and TM polarization) is shown in Figure 1b. The -1st order diffraction efficiency is given by the black curve. The requested efficiency specification is given by the dashed black line. The first diffraction order achieves peak efficiencies up to 70% in the VIS and it still provides 60% and 45% at the blue (340nm) and red (1040nm) edges of the spectrum.

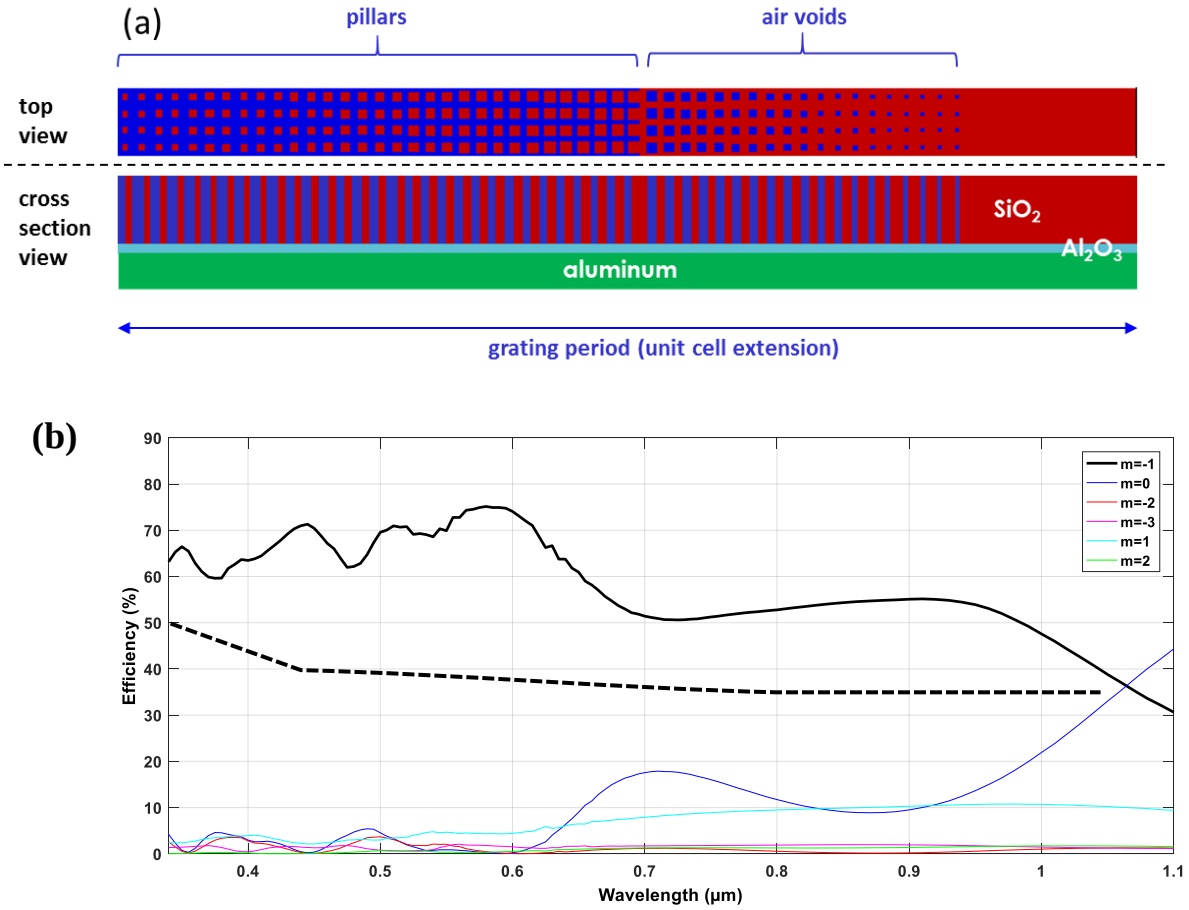

Figure 1. Sketch of geometrical layout of the grating's subwavelength features. b) Diffraction efficiency in -1st diffraction order under normal incidence (black). All other curves represent efficiencies of other diffraction orders and the dashed black line corresponds to the specification limit.

3. GRATING MANUFACTURING

We use electron-beam lithography and reactive ion etching (RIE) to realize surface relief structures on bulky substrates[8,9,10]. The substrate material is silicon, but it might be also other materials as long as the surface is coated with SiO_2. The main process flow is depicted in Figure 2. The substrate is coated by a metal mask (Cr) which is again coated by an electron sensitive resist. The resist is exposed to electron beam radiation which defines the binary grating pattern. Two subsequent dry RIE-process are used to i) transfer the resist pattern into the metal mask and ii) to transfer the metal mask pattern into the underlying SiO_2 material.

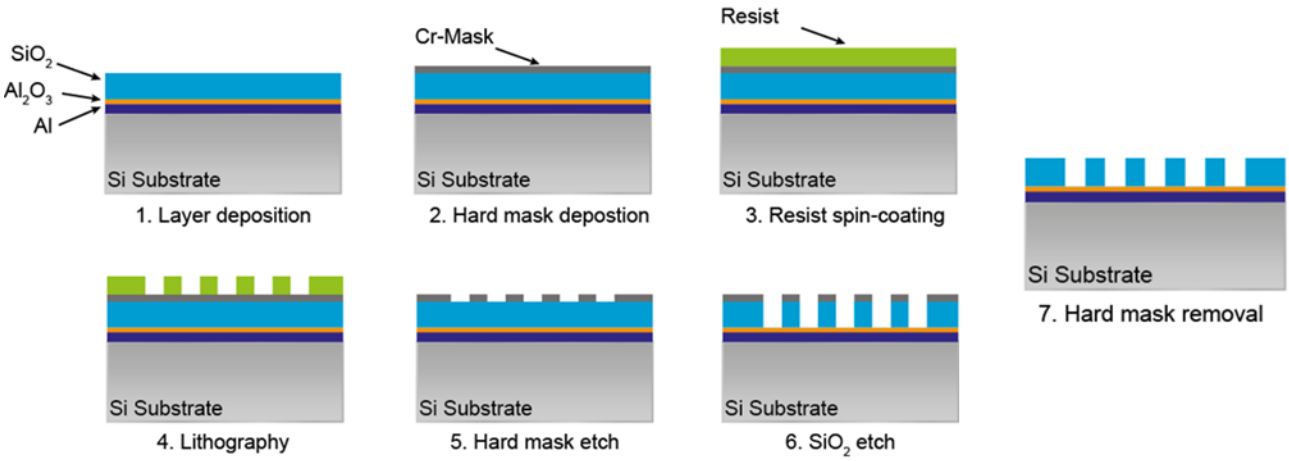

Figure 2. Manufacturing process flow for flat binary surface relief gratings by e-beam lithography and reactive ion etching.

The entire manufacturing process is monitored and controlled by various inspection methods, e.g. SEM (Scanning Electron Microscope) and AFM (Atomic Force Microscopy). This allows verifying and eventually correcting for correct feature size and depth level. Figure 3 shows an SEM image of the grating structure.

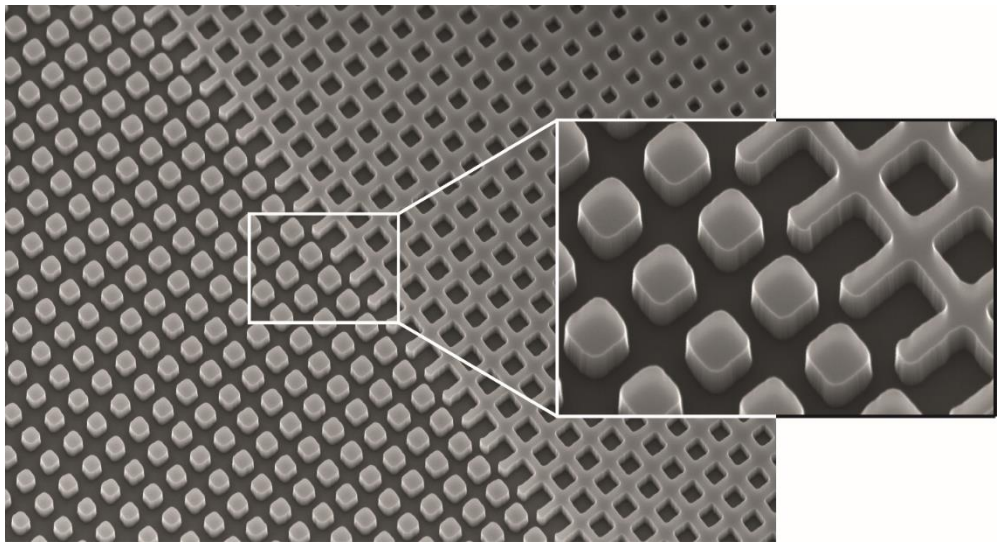

Figure 3. Top view of the gratings nanostructure achieved by SEM inspection. The image shows electron beam resist layer on top of the chromium hard mask layer.

One can nicely observe the tiny sub-wavelength features – pillars to the left and voids to the right where the gradient in feature size (diameter) is best visible for the air voids. Their size decreases in direction of the uppermost corner of the image.

After realization of a series of test grating samples which were used to develop and optimize the manufacturing processes, e.g. to meet the size constraints of all individual features, a full-size grating with a circular aperture of 80mm was realized on a silicon substrate. Figure 4 shows the photograph which demonstrates the high uniformity of the manufactured prototype.

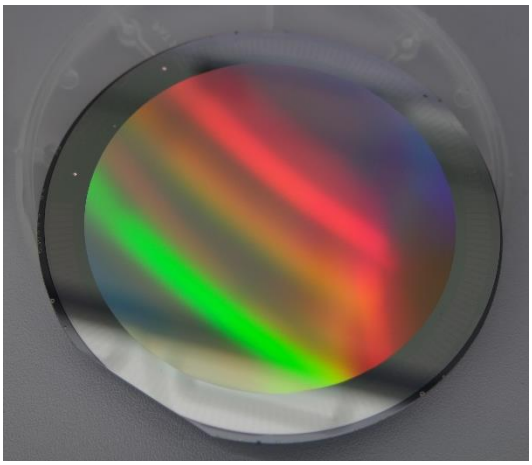

Figure 4. Photograph of a full-size prototype. The structured area has a diameter of 80mm.

4. GRATING OPTICAL CHARACTERISATION

The 80mm diameter binary blazed grating was characterized optically. We have measured diffraction efficiency and reflected wavefront accuracy.

The efficiency measurements were performed using a tunable light source. Thus, the grating is illuminated by a monochromatic light beam (diameter: ~3mm) with adaptable wavelength. The diffracted light is detected using an integrating sphere which is mounted on a goniometer setup. This allows to adjust the angle of diffraction with varying wavelength and thus guarantees to block light propagating in other diffraction orders. The results are shown in Figure 5. For comparison reasons, Figure 5 also provides the theoretical efficiency (red curve; according to the associated nominal grating layout). Despite some local differences (most likely attributed to manufacturing tolerances) it nicely follows the measured values.

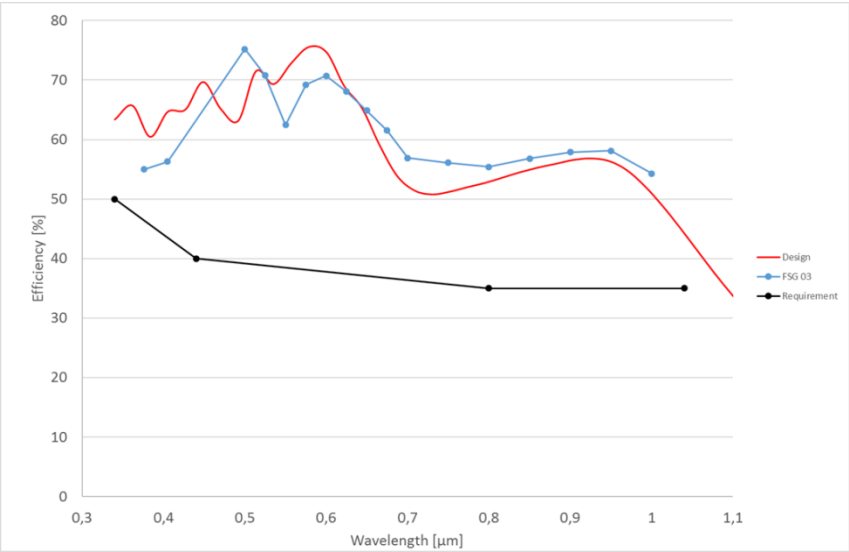

Figure 5. Diffraction efficiency of the prototype flat grating. The measurement results are provided by the blue symbols and the blue lines serve only to guide the eye. For comparison, the red curve shows the theoretical values according to the design. The black curve is the specification limit.

The data presented in Figure 5 corresponds to the spatial average throughout the entire structured area with diameter 80mm. The grating is mounted on an x/y-stage and actually allows for a spatially resolved measurement. An impression of that can be seen in Figure 6 which again verifies the high large-scale uniformity of the manufactured nano-structure.

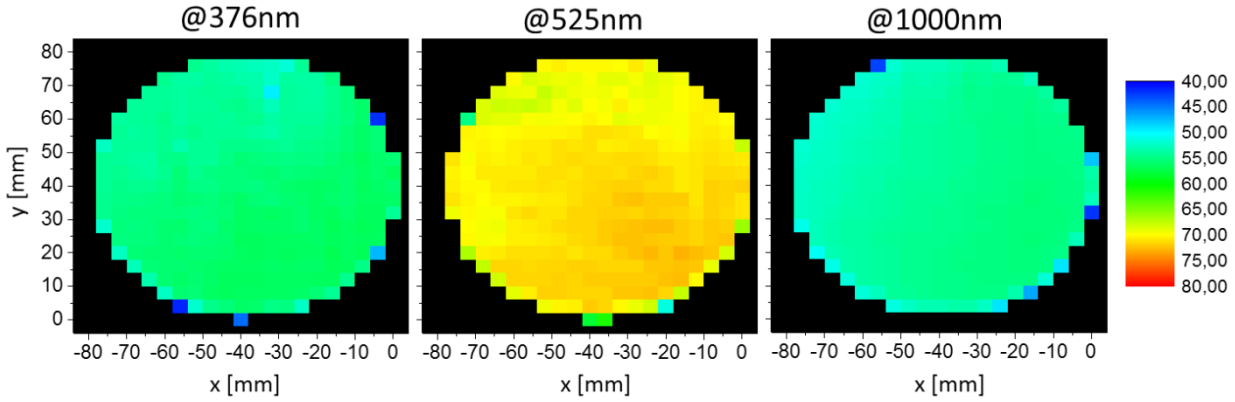

Figure 6. Spatial mapping of the diffraction efficiency in -1st order of the prototype flat grating for three different wavelengths, i.e. 376nm, 525nm, 1000nm. The mapping is performed throughout the structured area.

Figure 7 presents the wavefront error introduced by the fabrication process. The peak-to-valley (PV) differences are limited to 30nm and they translate into 5.4nm RMS deviation. Any WFE caused by substrate deformation was removed by measuring in -1st and +1st diffraction order and calculating the difference of both. Most likely, the real lithographically induced WFE is even smaller since the measured value already goes to the accuracy limit of the used interferometer.

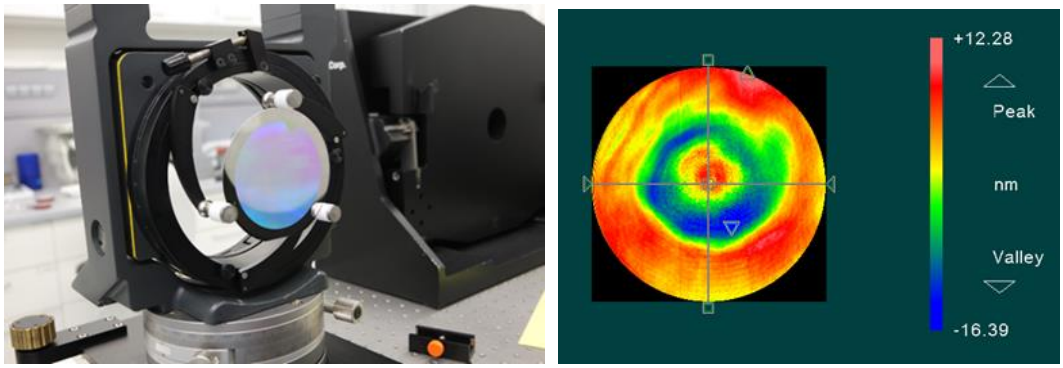

Figure 7. a) Prototype grating mounted within the interferometric measurement setup. b) Reflected wave-front error of the prototype grating where substrate induced deformations are not accounted for.

5. OUTLOOK TO CURVED SUBSTRATES AND LARGER BANDWIDTH

Since modern hyperspectral instruments[1] try to cover the entire bandwidth from the UV (340nm) up to the SWIR (2500nm) there is a large interest in dispersing elements, which exhibit an acceptable throughput within this region. In particular, gratings (either on plane or curved substrates) that operate in a single diffraction order throughout the entire bandwidth (we call this ultra-broadband operation) will pave the way for entirely new designs of the optical instrumentation.

5.1 Gratings on Curved Substrates

Nanoimprint technique has been investigated as a new manufacturing technique to provide (1) small series of gratings (2) curved gratings.

E-beam lithography has already proven to be a suitable technique to achieve the accuracy required for subwavelength gratings. However, considering the high feature density of the structures (for instance, more than 100 million of features per cm² for the manufactured grating), this technique is quite time-consuming, even for small-series manufacturing. We investigate nanoimprint technology (NIL) as an alternative lithography technique ensuring the same high resolution, with reduced process time (typically few minutes per wafer vs few hours).

The approach for the realization of the sub-wavelength grating structure based on NIL follows the previously described process (Figure 2), with the only difference that NIL replaces e-beam lithography for the step n°4. The soft UV-NIL technique we report about in this paper consists in fabricating a polymer stamp which will enable the replication of the nanometric patterns at the wafer-scale, several times, with a high reproducibility. The polymer stamp is previously produced from a flat silicon master mold fabricated with e-beam lithography and can be used for several replications. Hence, through the use of NIL, a single e-beam lithography leads to the production of several gratings with a high reproducibility.

The nanoimprint-based gratings are illustrated in Figure 8. We use the Surface Conformal Imprint Lithography (SCIL) module from Süss Microtec, which ensures a good uniformity for the application of stamp thanks to a sequential contact. A flexible transparent polymer stamp (PDMS) is fixed on a rigid and thin glass plate (200µm) and applied on a photosensitive resist under UV light (UV400), leading to pattern replication. The full process flow has then been performed to achieve the realization of the grating.

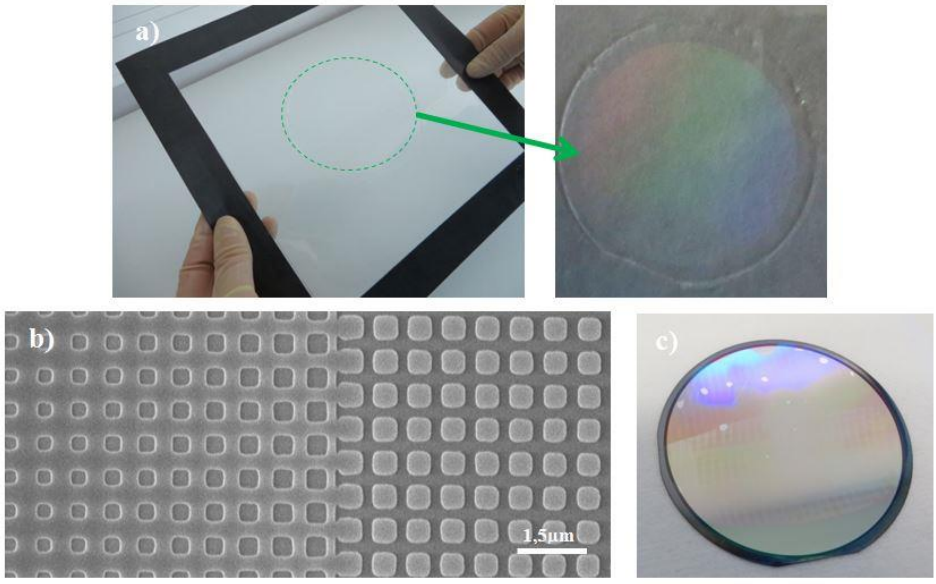

Figure 8. a) A SCIL stamp. b) Replicated patterns in the NIL resist. c) Grating manufactured by SCIL and plasma etching on a 3inch-wafer.

To check the ability of the nanoimprint technology to address curved substrate, we have carried out manual replication for applying the soft stamp onto the curved substrate. Photographs showing the outputs of the preliminary tests are given in Figure 9. The optimization of the process to ensure a good uniformity is under investigation and constitutes the main manufacturing challenge for the next generation of gratings.

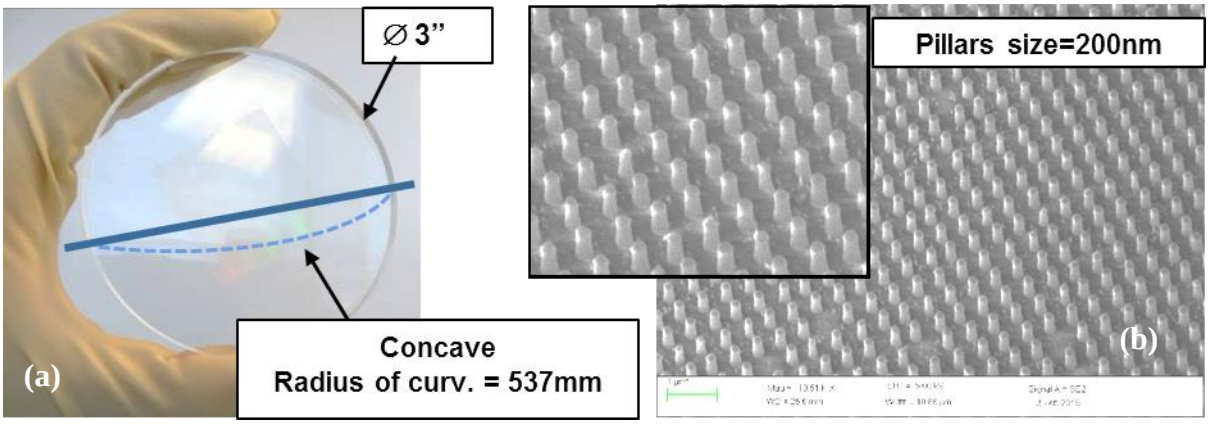

Figure 9. Preliminary tests: 3x3cm² grating (200nm-wide pillars) on a concave spherical fused silica substrate (R=537mm). (a) Photograph after “manual” nanoimprint replication. (b) SEM image of pillars after plasma etch in fused silica.

5.2 Ultra-broadband operation

The starting point is again the grating design concept as already introduced in Section 2. In particular, we assume a series of independent binary sub-wavelength features which vary in size throughout the grating’s unit cell. The ability for ultra-broadband operation is then verified by a dedicated grating design procedure. Using numerical optimization routines with an adapted merit function (maximum integrated throughput from UV to SWIR) allows to find a new configuration of sub-wavelength grating features with adapted size, pitch and depth. Figure 10 shows the outcome of such optimization where emphasis was put on a high throughput in the UV region. The threshold is to stay above 50% efficiency in the UV region which slightly goes on the costs of the achievable efficiency at the long-wavelength limit (SWIR). Nevertheless, this example shows the high potential of the selected grating geometry which can indeed be driven to meet the requirements for ultra-broadband operation. Due to the sole operation in 1st diffraction order the spectral signal shows no overlap in the angular domain such that cross-dispersing elements (as they are known e.g. from echelle spectrographs) are not required.

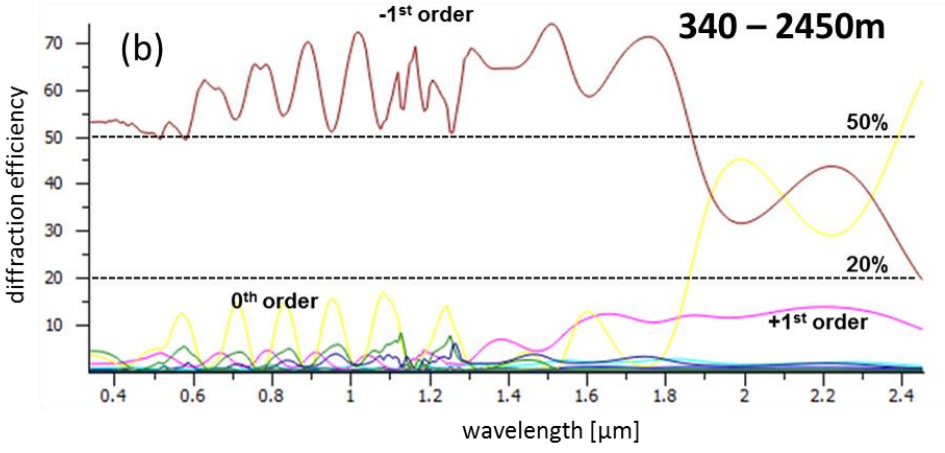

Figure 10 Calculated diffraction efficiency of “ultra-broadband” binary blazed gratings, after optimization for ultra-broadband operation between 340nm and 2450nm.

Another way using binary blazed gratings to tailor the efficiency spectral behavior for ultra-broadband operation is to design the grating to operate under 2 orders of diffraction. This principle can be found using standard échelette gratings: the -1 order is dedicated for long wavelength and the -2 order is dedicated for the shorter wavelength. The advantage of the binary blazed grating is its ability to tune the artificial material dispersion in order to achieve larger spectral behaviour for each order. Figure 11 shows an example of calculated diffraction efficiencies in the -1 and -2 orders as a function of the wavelength.

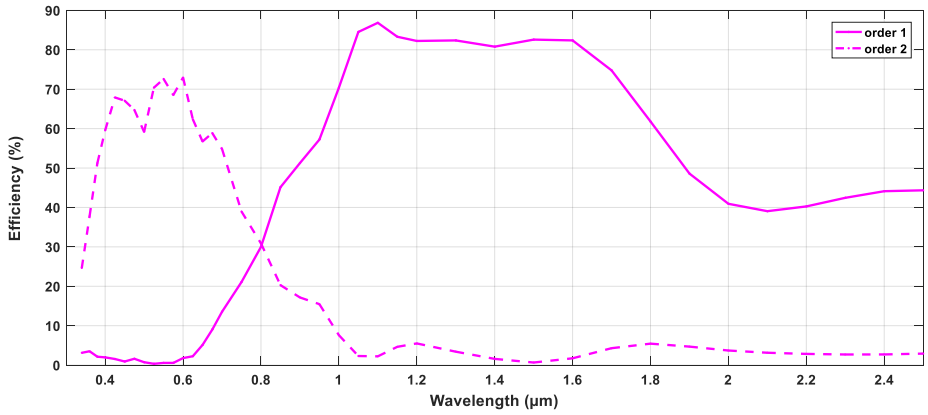

Figure 11. Calculated diffraction efficiency of "ultra-broadband" binary blazed grating operating under order-1 in the long wavelengths and under order-2 in the short wavelengths.

A third way to tune the efficiency spectral behavior is to design multiple-blaze subwavelength binary gratings. An example is a binary double-blaze grating operating in 400nm-1200nm. The period of the grating is around 16µm and it combines 2 alternative zones composed of subwavelength structures. Each zone is composed of particular variation of the subwavelength geometries.

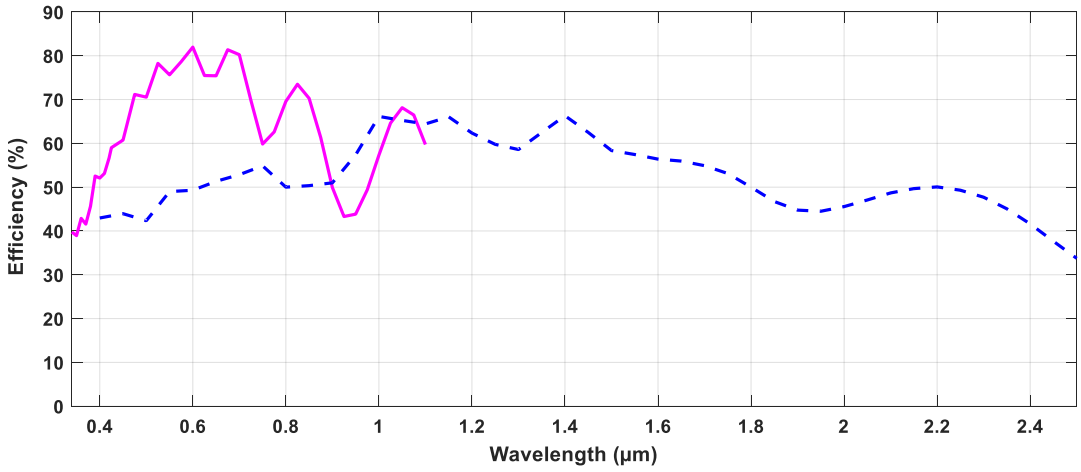

Figure 12. Calculated diffraction efficiency of binary multi-blazed gratings. The magenta curve corresponds to a 16µm period binary double blazed grating designed at 340nm-1.1µm. The dashed blue line corresponds to a preliminary estimated target for a 30µm period multi-blaze grating for an ultra-broadband operation.

The two zones are optimized for 500nm and 850nm operation. The calculated efficiency is given in Figure 12 by the magenta curve. This design was carried out for 400nm-1100nm operation, however this multiple blaze concept can be

extended to tailor the efficiency for ultra-broadband operation. The blue dashed line represents a preliminary estimated efficiency target for a 30µm period grating over the 400nm-2500nm band.

6. SUMMARY AND ACKNOWLEDGEMENT

In this paper, we demonstrated the design, realization and characterization of wide band reflective gratings operating under 340nm-1040nm. The manufactured prototype (of 80mm diameter) demonstrates efficiencies in between 55% and 75% and a WFE of 5.4nm RMS. The manufacturing process via electron beam lithography guarantees high wavefront-accuracy and a perfect control over size and shape of the sub-wavelength entities. We also show that this family of diffractive grating offers several degrees of freedom for the design of gratings for ultra-broadband applications. This work has concerned reflective gratings but it is applicable to transmission gratings, too. The extension of the technology to address binary blazed gratings on curved substrates is under investigation and will be the challenge for the next generation of gratings.
Part of this work was performed in the frame of the activity "Wide Band and High Efficiency Reflective Grating" under the TRP program funded by the European Space Agency.

REFERENCES

[1] Kaufmann, H., et al., "Science Plan of the Environmental Mapping and Analysis Program (EnMAP)," <http://doi.org/10.2312/enmap.2016.006> (16 August 2018).
[2] <https://hyspiri.jpl.nasa.gov/> (16 August 2018)
[3] Nieke, J, Rast M., "Towards the Copernicus Hyperspectral Imaging Mission For The Environment (CHIME)," Int. Geoscience and Remote Sensing Symposium, July 22-27, 2018
[4] Tetaz, N., Ruilier, C., Taccola, M., Viard, T., Lee Bouhours, M.-S.-L., Loiseaux, B., and Lehoucq, G., "Advanced large FOV UV/VIS/NIR/SWIR spectrometers for future earth observation instruments," Proc. SPIE 10563, 1056333 (2017)
[5] Liu, C., Straif, C., Flügel-Paul, T., Zeitner, U.D., and Gross, H., "Comparison of hyperspectral imaging spectrometer designs and the improvement of system performance with freeform surfaces," Appl. Opt. **56**, 6894-6901 (2017)
[6] Sauvan, C., Lalanne, P., and Lee, M.-S.-L., "Broadband blazing with artificial dielectrics," Opt. Lett. 29, 1593-1595 (2004)
[7] Ribot, C., Lee, M.-S.-L., Collin, S., Bansropun, S., Plouhinec, P., Thenot, D., Cassette, S., Loiseaux, B., and Lalanne, P., "Broadband and Efficient Diffraction," Adv. Opt. Mat. 1, 489-493 (2013)
[8] Zeitner, U.D., Oliva, M., Fuchs, F., Michaelis, D., Benkenstein, T., Harzendorf, T., and Kley, E.-B., "High performance diffraction gratings made by e-beam lithography," Apl. Phys. A 109, 789-796 (2012)
[9] Stork, W., Streibl, N., Haidner, N., and Kipfer P., "Artificial distributed-index media fabricated by zero-order gratings", Optics Letters, Vol. 16, Issue 24, pp. 1921-1923 (1991).
[10] Zeitner, U.D., Fuchs F., Kley, E.-B., and Tünnermann A., "High-refractive-index gratings for spectroscopic and Laser applications," Proc. SPIE **8995**, 899504 (2014)
[11] Flügel-Paul, T., Kalkowski, G., Benkenstein, T., Harzendorf, T., Matthes, A., and Zeitner, U. D., "New grating concepts in the NIR and SWIR spectral band for high resolution earth-observation spectrometers," Proc. SPIE 9912, 99122A (2016)